A Grand Scan of the pMSSM Parameter Space for Snowmass 2021

Jennet Dickinson[1], Samuel Bein[2], Sven Heinemeyer[3], Joshua Hiltbrand[4], Jim Hirschauer[1], Elliot Lipeles[5], Malte Mrowietz[2], and Nadja Strobbe[4]

[1]Fermi National Accelerator Laboratory
[2]University of Hamburg
[3]Cantabria Institute of Physics
[4]University of Minnesota
[5]University of Pennsylvania

March 2022

1 Introduction

It is well known that the Standard Model of particle physics (SM) cannot be the ultimate theory of fundamental particles and interactions. Most obviously, the SM does not incorporate gravity and explains neither the identity of the astronomically observed dark matter (DM) nor the observed multiplicities and hierarchies of interactions, flavor, and fermion generations. Of the many models proposed to address the shortcomings of the SM, supersymmetry (SUSY) garners significant interest because it simultaneously explains the finite mass of the recently discovered Higgs particle, provides a DM candidate, and allows more precise unification of the forces.

The minimal supersymmetric standard model (MSSM) has 120 parameters describing particle masses and interactions. In order to facilitate interpretation of experimental results within the MSSM framework, these 120 free parameters have traditionally been reduced to five, by assuming relationships between MSSM parameters based on a choice of the SUSY breaking mechanism at high energy scale, in the form of the constrained MSSM (cMSSM) [1–4] or two parameters, by assuming pair production of a single SUSY particle (sparticle) with fixed decay chain, in the form of simplified model spectra (SMS) [5–7]. While these frameworks allow for efficient interpretation of results, they do so at the expense of sampling only a very small part of the phase space of the MSSM and potentially focusing on signatures that may not be realized in nature.

Recently, the ATLAS and CMS collaborations and theorists have attempted to ameliorate the limitations of interpretations based on the cMSSM and SMS by use of the phenomenological MSSM (pMSSM) [8–13], which reduces the 120-parameter MSSM space to 19 free parameters, specified at the electroweak (EW) scale, based on assumptions related to current experimental constraints (including those from flavor, CP violation, and EW symmetry breaking) rather than details of the SUSY breaking mechanism. The parameters of the pMSSM and their definitions are listed in Table 1.

Building on the methods of the CMS and ATLAS collaborations, we have developed a flexible framework for interpretation of SUSY sensitivity studies for future colliders in the framework of the pMSSM. We perform a grand scan of the pMSSM parameter space that covers the logical OR of accessible ranges of many collider scenarios, including electron, muon, and hadron colliders at a variety of center of mass energies. This enables comparisons of sensitivity and complementarity of different future experiments, including both colliders and precision measurements in the Cosmological and Rare Frontiers. The pMSSM parameter ranges considered are listed in Table 1. The lower bounds on each parameter are chosen based on experimental constraints and phenomelology considerations. The upper bounds are chosen to be within reach of the sensitivity of a 100 TeV pp collider.

The output of the scan for each selected scan point includes the pMSSM parameter values, SUSY particle masses, calculated values of observables included in the scan likelihood (e.g. top and bottom quark masses,

Param.	Definition	Range
M_A	mass of psuedoscalar Higgs boson	100 GeV - 25 TeV
$\tan\beta$	ratio of Higgs vevs	1 - 60
$\lvert\mu\rvert$	Higgs-higgsino mass parameter	80 GeV - 25 TeV
$\lvert M_1\rvert$	bino mass parameter	1 GeV - 25 TeV
$\lvert M_2\rvert$	wino mass parameter	70 GeV - 25 TeV
M_3	gluino mass parameter	200 GeV - 50 TeV
$m_{\tilde{L}^{1,2}}$	$1^{\text{st}}/2^{\text{nd}}$ gen. left-handed slepton mass	90 GeV - 25 TeV
$m_{\tilde{R}^{1,2}}$	$1^{\text{st}}/2^{\text{nd}}$ gen. right-handed slepton mass	90 GeV - 25 TeV
$m_{\tilde{L}^3}$	3^{rd} gen. left-handed slepton mass	90 GeV - 25 TeV
$m_{\tilde{R}^3}$	3^{rd} gen. right-handed slepton mass	90 GeV - 25 TeV
$m_{\tilde{q}^{1,2}}$	$1^{\text{st}}/2^{\text{nd}}$ gen. left-handed squark mass	200 GeV - 50 TeV
$m_{\tilde{u}^{1,2}}$	$1^{\text{st}}/2^{\text{nd}}$ gen. right-handed u-type squark mass	200 GeV - 50 TeV
$m_{\tilde{d}^{1,2}}$	$1^{\text{st}}/2^{\text{nd}}$ gen. right-handed d-type squark mass	200 GeV - 50 TeV
$m_{\tilde{q}^3}$	3^{rd} gen. left-handed squark mass	100 GeV - 50 TeV
$m_{\tilde{u}^3}$	stop quark mass	100 GeV - 50 TeV
$m_{\tilde{d}^3}$	sbottom quark mass	100 GeV - 50 TeV
$\lvert A_\tau\rvert$	τ trilinear coupling	1 GeV - 7 TeV
$\lvert A_b\rvert$	bottom trilinear coupling	1 GeV - 7 TeV
$\lvert A_t\rvert$	top trilinear coupling	1 GeV - $3(m_{\tilde{q}^3}m_{\tilde{u}^3})^{1/2}$

Table 1: The 19 parameters of the pMSSM and their allowed ranges in the Snowmass 2021 scan.

B meson branching fractions, etc.), and calculated values of observables not included in the scan likelihood (e.g. the dark matter relic density). The scan also prodcues an SLHA file [14] for generating simulated events for each point. Event generation and detector simulation is not discussed in this whitepaper.

Section 2 describes how the scan is performed by using a Markov chain Monte Carlo procedure to sample points from the 19-dimensional pMSSM parameter space. Section 3 describes how properties of theoretical and experimental interest are calculated for each point. Section 4 reviews the scan coverage in terms of interesting physics processes and estimates the impact of future precision measurements on the pMSSM phase space. Conclusions are drawn in Section 5.

2 Markov chain Monte Carlo sampling procedure

Due to the high dimensionality of the pMSSM and the large span of the parameter ranges (Table 1), the parameter space considered in this scan is extremely large. A Markov chain Monte Carlo (McMC) [] algorithm is therefore used to explore the space in a sophisticated way, guided by a likelihood constructed from existing experimental results (see Section 2.1)

To begin the McMC scan, an initial pMSSM point in the 19D parameter space is selected at random within the ranges specified in Table 1. The SPheno 4.0.5 [15, 16] spectrum generator is used to calculate the corresponding particle masses and decays. The Higgs sector is then replaced with that calculated by FeynHiggs 2.18.0 [17–24]. If SPheno or FeynHiggs indicate that the selected point is not a valid pMSSM model, a new random point is selected until a viable initial point is obtained. The McMC likelihood for the initial point is calculated as described in Section 2.1.

The following steps are repeated until the desired number of points is reached:

1. A new pMSSM point $\vec{x}'$ is selected from the previous one ($\vec{x}$) by sampling randomly from the probability distribution given by the stepping functions $f_i(x_i)$. The form of the stepping function is discussed in detail in Section 2.2.

2. If the pMSSM point does not fall within the ranges listed in Table 1, return to step 1.

3. The particle spectrum and Higgs sector for $\vec{x}'$ are calculated with SPheno and FeynHiggs respectively. If the pMSSM point is not a valid model, return to step 1.

4. Run additional calculations required to compute the McMC likelihood (detailed in Section 2.1).

5. If the likelihood ratio $L(\vec{x}')/L(\vec{x}) > 1$, the point is accepted. If the likelihood ratio $L(\vec{x}')/L(\vec{x}) \leq 1$, it is tested against a random number in the interval [0,1], and the point is accepted if $L(\vec{x}')/L(\vec{x}) > 0$ (this allows the McMC to move away from a local minimum). Otherwise, the point is rejected.

6. If the point is rejected, return to step 1.

7. If the point is accepted, save the point. Then take $\vec{x} = \vec{x}'$ and repeat from step 1.

The total pMSSM scan is comprised of the union of 400 independent McMC scan threads, each starting from a different initial point.

2.1 Construction of the likelihood

In order to steer the Markov chain Monte Carlo out of regions of parameter space that are well excluded by existing measurements, a likelihood function is constructed that incorporates the following:

- Measurements of top and bottom quark masses
- Measurements of the strong coupling constant α_S
- Measured branching ratios of $B \to \tau\nu$, $D_s \to \tau\nu$, and $D_s \to \mu\nu$
- Measurements of B-physics observables from Superiso [25]
- LHC Higgs boson measurements from HiggsSignals [26] and HiggsBounds [27–30]
- Measurement of Δa_μ from the muon $g-2$ experiment (in half of scan threads, see below)

The total likelihood is taken to be a product of the contribution from each of these sources. The likelihood does not include the following observables, though their values are computed for each point to allow understanding of how the allowed pMSSM space relates to physical observables of interest.

- Dark matter relic density
- Identity of lightest SUSY particle (LSP)
-

Each of the observables listed in Table 2 has a Gaussian contribution to the total likelihood, with the mean and width corresponding to the measured value and uncertainties, respectively. The values of these observables are calculated by SPheno for each sampled pMSSM point. The contribution of each observable to the total likelihood the Gaussian likelihood function evaluated at the value calculated by SPheno.

Observable	Measurement
m_t	173.1 ± 0.9 GeV
m_b	$4.18^{+0.03}_{-0.02}$ GeV
α_s	0.1181 ± 0.0011
$BR(B \to \tau\nu)$	$(1.09 \pm 0.24) \times 10^{-4}$
$BR(D_s \to \tau\nu)$	$(5.48 \pm 0.23) \times 10^{-2}$
$BR(D_s \to \mu\nu)$	$(5.49 \pm 0.16) \times 10^{-3}$

Table 2: Experimental results with Gaussian contribution the McMC likelihood, from the Particle Data Group [31].

The difference between the standard model value and the pMSSM value for the anomalous muon magnetic moment, Δa_μ, is calculated for each point by the GM2Calc package [32, 33]. In order to allow for sufficient statistics near both the SM value of $\Delta a_\mu = 0$ and the measured central value of $\Delta a_\mu = 251 \times 10^{11}$ [34], Δa_μ

is included in the likelihood for only half of the scan threads. When included in the likelihood, the Δa_μ contribution is taken to be Gaussian with mean corresponding to the measured central value, with the same value (251×10^{-11}) used for the width. This approach ensures that pMSSM regions near the measured value and the SM prediction are both populated by the scan.

For each sampled pMSSM point, the Superiso 4.1 package [25] is used to calculate the values of B-physics observables from the spectrum provided by SPheno. Superiso also provides the compatibility of the calculated observables with existing measurements in the form of a χ^2, which is incorporated into the likelihood according to

$$L = \frac{(\chi^2)^{(\frac{n}{2}-1)}}{2^{\frac{n}{2}}\Gamma(\frac{n}{2})} e^{-\chi^2/2} \tag{1}$$

where n is the number of degrees of freedom. The B-physics observables included in the Superiso χ^2 are listed in Table 3, corresponding to $n = 9$.

Observable	n_{dof}
$\Delta_0(B \to K\gamma)$	1
$BR(B^0 \to K^{*0}\gamma)$	1
$BR(B_s \to \mu\mu)$	1
$BR(B_d \to \mu\mu)$	1
$BR(b \to s\gamma)$	1
$BR(b \to s\mu\mu)$	2
$BR(b \to see)$	2

Table 3: B-physics observables included in the calculation the χ^2 from Superiso. For the last two rows, measurements from two energy regions are included.

HiggsSignals 2.6.0 [26] is then used to calculate each point's compatibility with LHC Higgs measurements, including measurements of the Higgs boson mass. HiggsSignals returns a χ^2 value, which is incorporated into the total likelihood according to Equation 1 with number of degrees of freedom $n = 107$. The likelihood corresponding to $A \to \tau\tau$ searches at the LHC is calculated by HiggsBounds 5.9.1 [27–30] and included in the total McMC likelihood.

2.2 Stepping in the McMC

Given pMSSM point $\vec{x}$, the stepping functions $f_i(x_i)$ are the probability distributions from which the next pMSSM point is chosen. Two forms are considered for the stepping functions in the pMSSM scan. The first is denoted **linear**:

$$f(x_i) = \text{Gaus}(\mu = x_i, \sigma = \sigma_0 \times w) \tag{2}$$

Here, w is the width of the parameter range allowed for parameter x_i (see Table 1), and σ_0 is a tunable step size parameter. The second stepping function is denoted **logarithmic**:

$$f(x_i) = \exp\left[\text{Gaus}(\mu = \ln|x_i|, \sigma = \sigma_0 \times w)\right] \tag{3}$$

where w and σ_0 have the same meanings as above.

Because the logarithmic stepping function is positive definite, each new point selected from this distribution will have positive sign. However, some pMSSM parameters can have negative values (M_1, M_2, μ, A_t, A_b, A_l). The sign of each parameter is therefore fixed to that of the randomly selected initial point, and the magnitude only is determined by the stepping function. The final combination of many scans with different initial points will insure all sign combinations are explored.

Relative to the linear stepping function, the logarithmic stepping function ensures that lower parameter values are explored with finer granularity than higher ones. This has several advantages for the pMSSM scan. First, the highest parameter values are inaccessible to many collider scenarios of interest for Snowmass 2021, and the use of log stepping in some or all parameters ensures that the scan is not overwhelmed by points

only accessible at a 100 TeV proton−proton collider. Second, at lower sparticle masses, the near-degeneracy between SUSY and SM particles yields a more diverse array of experimental signatures.

A series of small-scale (200,000 point) test scans are generated to optimize the choice of stepping functions. In these tests, the logarithmic stepping function is taken as the default for all pMSSM parameters, and four values of the step size are tested: $\sigma_0 = 0.05$, 0.10, 0.20, and 0.30. These scans are labelled by "Log σ_0" for the remainder of this section. An additional scan setup, "Lin 0.05", aims to sample a higher fraction of points where the strong SUSY sector is decoupled: here, the logarithmic stepping function ($\sigma_0 = 0.05$) is used for all but the squark and gluino mass parameters, which instead employ the linear stepping function with $\sigma_0 = 0.05$.

The test scan setups are listed in the top section of Table 4. The middle section of this table reports the number of points sampled, accepted by the McMC, and accepted after post-processing (see Section 3), as well as the total efficiency.

	Log 0.05	Log 0.10	Log 0.20	Log 0.30	Lin 0.05
Stepping (squark, gluino)	log	log	log	log	lin
Stepping (other)	log	log	log	log	log
Step width σ_0	5%	10%	20%	30%	5%
Sampled points	200100	200100	200100	200100	200100
McMC accepted points	7938	3160	1541	1214	7728
Post-process accepted points	1045	408	161	119	2639
Total Efficiency	0.0052	0.0020	0.0008	0.0006	0.0132
Lightest squark mass $>$ 10 TeV	0.0775	0.1005	0.1988	0.1681	0.2865
Δm(LSP – gluino) $<$ 500 GeV	0.0057	0.0123	0	0	0.0072
Δm(LSP – stop) $<$ 500 GeV	0.0029	0	0	0	0.0023
Δa_μ within 1σ of meas.	0.0593	0.0760	0.0559	0.0588	0.0940

Table 4: Results of the test scans with different stepping configurations.

The lower portion of Table 4 shows the fraction of points in a few regions that are of special interest:

- Strong SUSY sector is decoupled: lightest squark or gluino mass $>$ 10 TeV
- Compressed mass spectra: Δm betweeen the lightest stable particle and the stop or gluino $<$ 500 GeV
- Δa_μ is within 1σ of the measured value of 251 ± 59

A high density of points in these regions is useful for Snowmass 2021 studies. Largely due to the 29% of points with lightest squark mass above 10 TeV, the Lin 0.05 test scan is deemed the most optimal and is used as the final stepping configuration.

Figure 1 shows the up-type squark mass distributions of points sampled (both accepted and rejected) by the McMC for the different stepping configurations. The change in σ_0 corresponds to a change in the slope of

In order to maximize the statistics of the final scan, the results of the four non-optimal test scans presented in this section are combined with the results of the final configuration. However, the contribution from these test scans is small, and the overall scan behavior follows that of Lin 0.05.

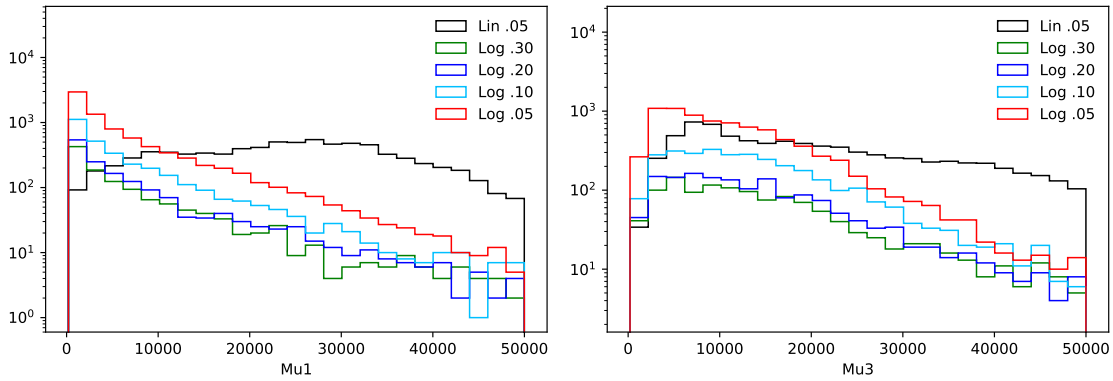

(a) 1st/2nd generation up-type squark mass parameter(b) 3rd generation up-type squark mass parameter [GeV] [GeV]

Figure 1: Up-type squark mass parameter of sampled pMSSM points accepted by the McMC, shown for different stepping configurations.

3 Selection of sampled points

Following the sampling of pMSSM points, a post-processing step is applied to further remove experimentally disfavored regions of the parameter space from the scan. In particular, points are rejected if they satisfy one or more of the following criteria:

- excluded at 95% CL by LHC Higgs searches, as calculated by HiggsBounds
- excluded at 95% CL by LHC SUSY searches, as calculated by SModelS [35–38]
- excluded at 95% CL by dark matter measurements, as calculated by MicrOMEGAs [39–41]

The HiggsBounds likelihood of the $A \to \tau\tau$ search is used directly in the McMC likelihood described above. However, the boolean HiggsBounds outputs, which indicate whether a point is excluded by LHC Higgs searches, is applied only at the post-processing stage. A pMSSM point is rejected if it is excluded at 95% CL by at least one of the four LHC Higgs searches with highest expected sensitivity to that point.

The exclusion limits from LHC simplified-model searches on each pMSSM point are calculated by SModelS 2.1 [35–38], which provides a boolean output indicating whether the point is excluded at 95% CL.

The MicrOMEGAs package [39] 5.2.7.a calculates exclusion limits from $Z \to$ invisible, LEP [40], dark matter mass limits and direct detection experiments [41]. Points excluded by any of these measurements at 95% CL are rejected. The dark matter relic density Ωh^2 is also calculated at the post-processing step by MicrOMEGAs. Though not included in the McMC likelihood, this observable can be used to further focus on regions of the pMSSM scan that are experimentally and theoretically motivated.

SOME TEXT describing Table 5.

	With Δa_μ	Without Δa_μ	Total
Sampled points	5,617,746		
McMC accepted points	61,240		
Post-process accepted points	9,438		
Total Efficiency	1.0%		
Squark, gluino masses > 10 TeV			
Δm(LSP, gluino) < 500 GeV			
Δm(LSP, stop) < 500 GeV			
Δa_μ within 1σ of meas.			

Table 5: Summary of the scanned pMSSM points.

4 Results

4.1 Higgs boson properties

The Higgs boson mass calculated by FeynHiggs is shown in Figure 2, with the measured best-fit value shown with a vertical black line, and the uncertainty with dashed lines. Since Higgs boson mass measurements are incorporated into the McMC likelihood through the HiggsSignals χ^2, the sampled points again peak near the measured value.

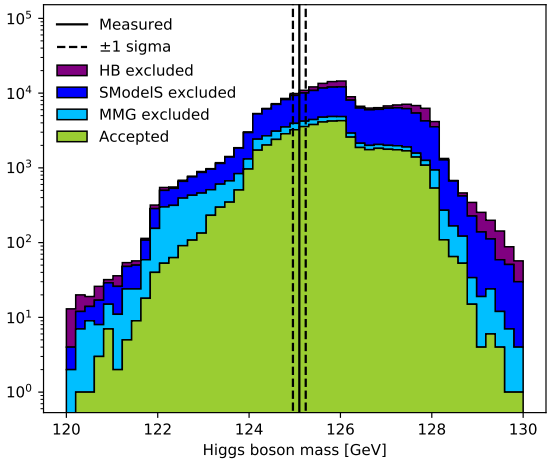

Figure 2: Higgs boson mass calculated by FeynHiggs for each pMSSM point, with the measured value and uncertainties indicated by vertical lines.

Higgs boson couplings for each pMSSM point are calculated by FeynHiggs and studied in the κ-framework, where for particle p with Higgs coupling λ_p

$$\kappa_p = \frac{\lambda_p}{\lambda_{\mathrm{SM}}} \tag{4}$$

The Higgs boson couplings to the top, bottom, and charm quark are shown for each pMSSM point in Figure 3. The Higgs boson couplings to the tau lepton and muon are shown in Figure 4. For all the fermions studied, the calculated coupling values peak sharply the expected SM value of $\kappa = 1$. This is consistent with the LHC measurements to date, which enter the McMC likelihood through the contribution from HiggsSignals.

The pseudo-scalar component of each Higgs-fermion coupling is also calculated, but is not found to deviate from zero in any of the sampled pMSSM points. This indicates that, should CP-violation be discovered in Higgs-fermion couplings, it is unlikely explainable by a SUSY model consistent with the pMSSM.

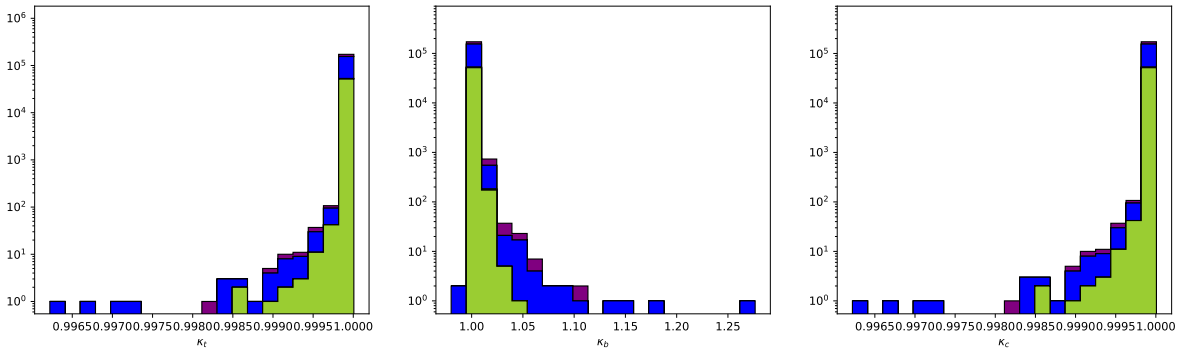

Figure 3: Higgs couplings κ_t, κ_b, and κ_c calculated by FeynHiggs for each pMSSM point.

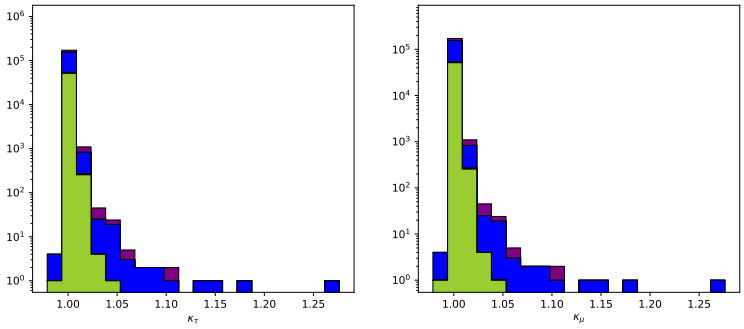

Figure 4: Higgs couplings κ_τ and κ_μ calculated by FeynHiggs for each pMSSM point.

Figure 5 shows the Higgs boson couplings to vector bosons. As for the fermions, the calculated coupling values peak sharply the expected SM value.

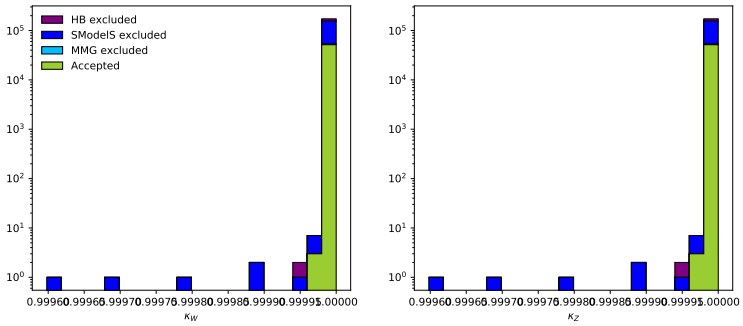

Figure 5: Higgs couplings κ_W and κ_Z calculated by FeynHiggs for each pMSSM point.

Measurement of the Higgs boson self-coupling κ_λ is a target for many future collider experiments. Unlike the Higgs couplings to fermions and vector bosons, the Higgs self-coupling is unconstrained in the McMC likelihood. As shown in Figure 6, the pMSSM scan populates a large range in κ_λ, with a peak near the SM value.

Some words about the precision measurements scheme and a reference to the paper from Caterina.

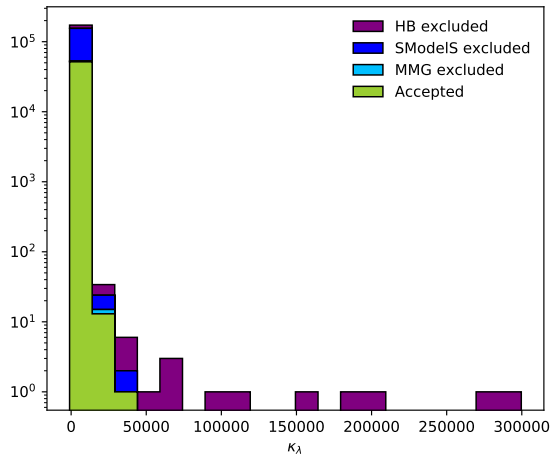

Figure 6: Higgs boson self-coupling calculated by FeynHiggs for each pMSSM point.

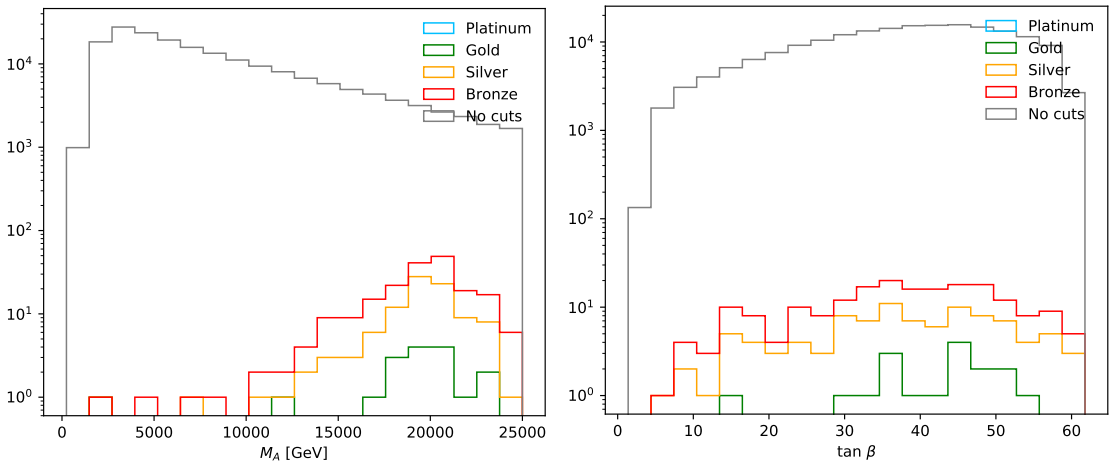

Figure 7: Higgs boson self-coupling for different cuts

4.2 Muon magnetic moment

Recent measurements of the anomalous muon magnetic moment Δa_μ [34] have sparked renewed interest in possible Beyond the Standard Model physics contributing to this observable. The McMC likelihood is therefore constructed to populate the region near the measured value as well as the Standard Model value ($\Delta a_\mu = 0$). The distribution of Δa_μ for the sampled pMSSM points, shown in Figure 8, exhibits the desired two-peak structure. Though much of the peak at the measured value is excluded by SModelS, approximately 10% of points passing all selection have Δa_μ within 1σ of the measurement (denoted by vertical lines).

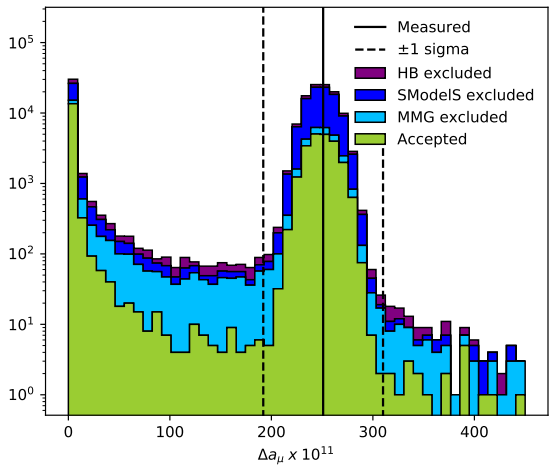

Figure 8: Distribution of Δa_μ for the sampled pMSSM points. The predicted Standard Model value corresponds to $\Delta a_\mu = 0$, and the measured central value and uncertainties indicated by vertical lines.

The distribution of pMSSM points satisfying the latest g-2

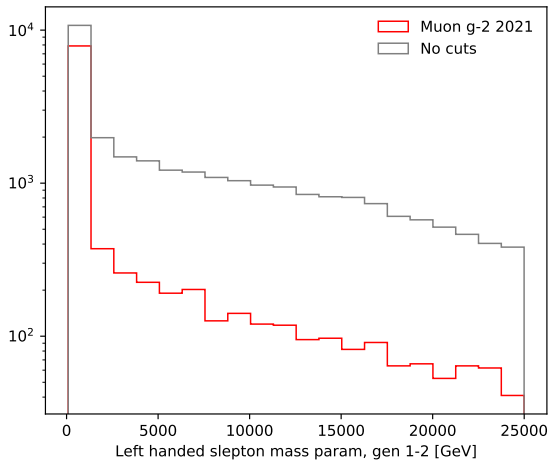

Figure 9: amu for different cuts

4.3 Electroweakino dark matter

The dark matter particle is taken to correspond to the lightest stable neutral particle (LSP) in the model, the neutralino χ_1^0. The dark matter relic density due to the LSP is calculated by MicrOMEGAs, is shown in Figure 10. The impact of LHC searches on these observables is quite pronounced: SModelS excludes the majority of points with very light dark matter candidates, and with very low relic density. The value of Ωh^2

measured by Planck [] is shown in the right-hand side of Figure 10. The pMSSM scan populates values of this parameter over a very wide range compared to the precision of the measurement.

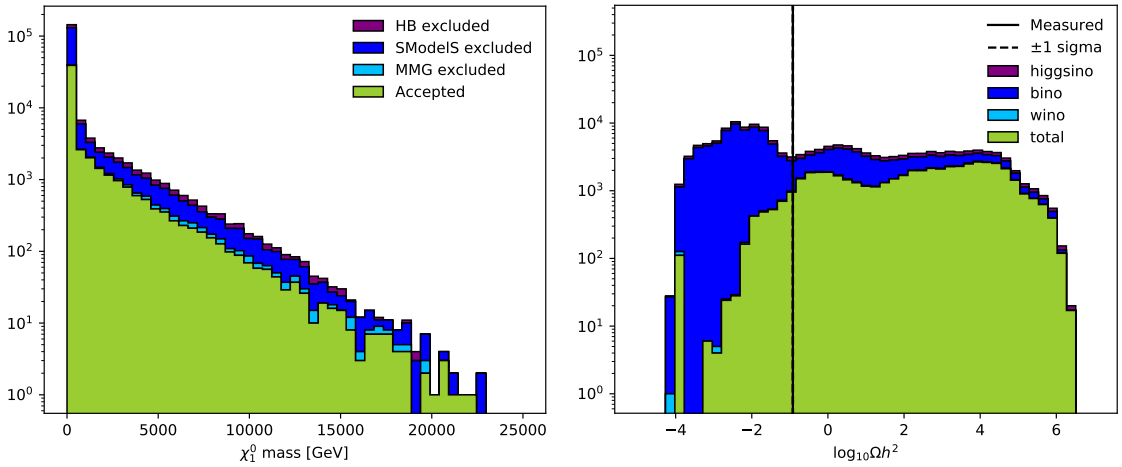

Figure 10: The LSP mass (left) and dark matter relic density (right) for each sampled pMSSM point. The measured value of Ωh^2 is indicated by vertical lines.

The LSP is a superposition of electroweakino states (bino, wino, and higgsino). The LSP composition in the sampled pMSSM points (after all selection is applied) is shown in Figure 11. The top left corner corresponds to pure wino, the bottom left to pure higgsino, and the bottom right to pure bino dark matter. Most pMSSM points contain an LSP that is relatively pure in the electroweakino composition, though the scan also captures points with a mixture.

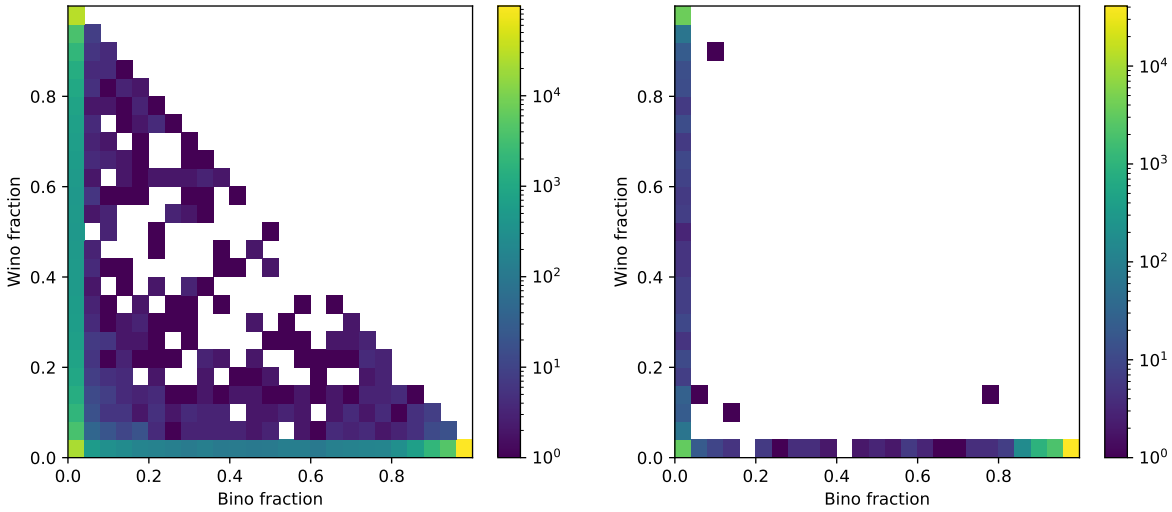

Figure 11: The electroweakino composition of the dark matter candidate in terms for each pMSSM point, (left) for points accepted by the McMC and (right) for points passing all post-processing selection. In each panel, the top left corner corresponds to pure wino, the bottom left to pure higgsino, and the bottom right to pure bino dark matter.

Each pMSSM point is then labelled by the electroweakino comprising the largest component of the LSP, thereby separating the scan into samples with bino-, wino-, and higgsino-like dark matter. The dark matter relic density for each component sample is shown in Figure 13. The sampled points with very high relic density are dominated by models with bino-like dark matter. Wino-like dark matter, on the other hand, is

	McMC accepted	Post-process accepted
Mostly wino	15,555	776
Mostly bino	28,874	8,083
Mostly higgsino	11,987	554
Mixed wino/bino	4	0
Mixed bino/higgsino	1,064	6
Mixed wino/higgsino	214	1

Table 6: DM candidate composition. Mostly ($> 80\%$) and Mixed ($> 40/40\%$)

concentrated at low values of Ωh^2 and comprises most of the low tail excluded by SModelS in Figure 10. Near the measured value of the relic density, wino-, bino-, and higgsino-like dark matter all contribute.

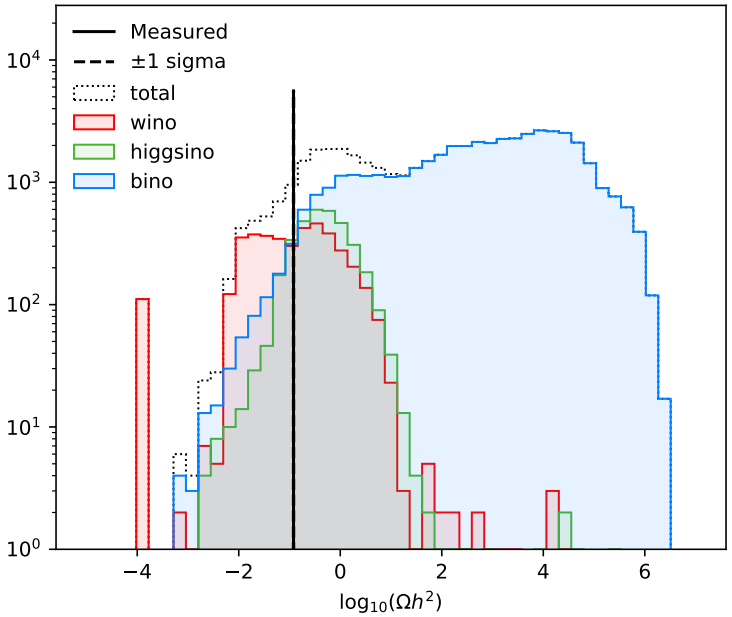

Figure 12: Distribution of the dark matter relic density for the sampled pMSSM points, after the full selection has been applied, broken down by the electroweakino composition of the dark matter candidate.

The two dimensional distribution in the space of the relic density and LSP mass is shown in Figure **??**.

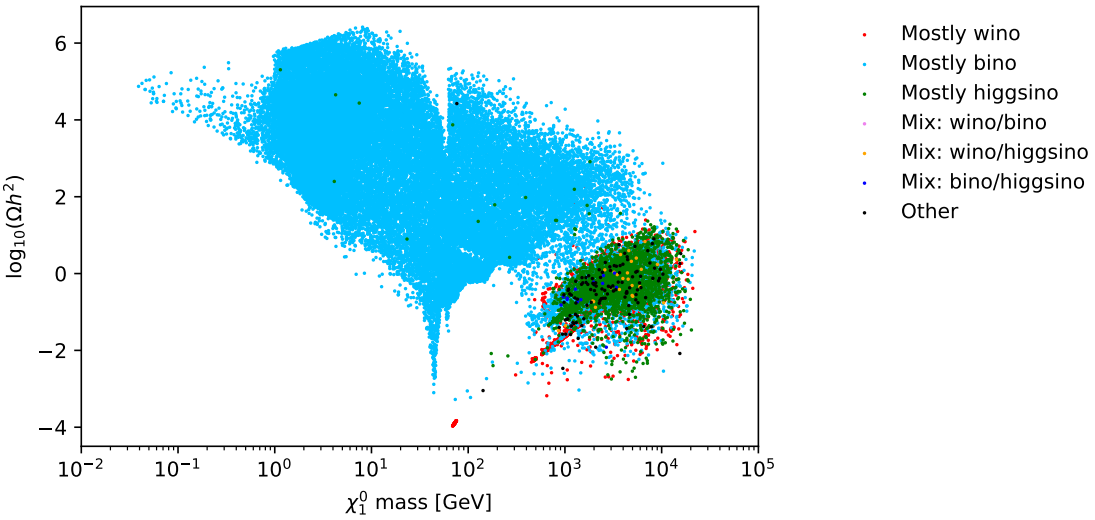

Figure 13: Distribution of the dark matter relic density for the sampled pMSSM points, after the full selection has been applied, broken down by the electroweakino composition of the dark matter candidate.

5 Conclusion

To be added.

With a large scan of the pMSSM completed, further studies that include event generation will require an additional slimming down of the sample to a tractable number of points. Scan points can be sampled with low density in less interesting regions, and high density in regions of particular interest.

Such interesting regions include, but are not limited to, points that have

- the strong SUSY sector decoupled (e.g. lightest squark mass > 10 TeV)
- Δa_μ near the measured value of $(251 \pm 59) \times 10^{11}$
- dark matter relic density consistent with observations from Planck []
- dark matter with specific electroweakino composition
- compressed mass spectra (e.g. LSP mass similar to the stop or gluino)

The final focus of the scan, including what pMSSM points are selected for event generation, will depend on the interests of the Snowmass 2021 community.

References

[1] Ali H. Chamseddine, Richard L. Arnowitt, and Pran Nath. "Locally Supersymmetric Grand Unification". In: *Phys. Rev. Lett.* 49 (1982), p. 970. DOI: 10.1103/PhysRevLett.49.970.

[2] Riccardo Barbieri, S. Ferrara, and Carlos A. Savoy. "Gauge Models with Spontaneously Broken Local Supersymmetry". In: *Phys. Lett. B* 119 (1982), p. 343. DOI: 10.1016/0370-2693(82)90685-2.

[3] Luis E. Ibanez. "Locally Supersymmetric SU(5) Grand Unification". In: *Phys. Lett. B* 118 (1982), pp. 73–78. DOI: 10.1016/0370-2693(82)90604-9.

[4] Lawrence J. Hall, Joseph D. Lykken, and Steven Weinberg. "Supergravity as the Messenger of Supersymmetry Breaking". In: *Phys. Rev. D* 27 (1983), pp. 2359–2378. DOI: 10.1103/PhysRevD.27.2359.

[5] Johan Alwall, Philip C. Schuster, and Natalia Toro. "Simplified models for a first characterization of new physics at the LHC". In: *Physical Review D* 79.7 (Apr. 2009). ISSN: 1550-2368. DOI: 10.1103/physrevd.79.075020. URL: http://dx.doi.org/10.1103/PhysRevD.79.075020.

[6] Daniele Alves et al. "Simplified models for LHC new physics searches". In: *Journal of Physics G: Nuclear and Particle Physics* 39.10 (Sept. 2012), p. 105005. ISSN: 1361-6471. DOI: 10.1088/0954-3899/39/10/105005. URL: http://dx.doi.org/10.1088/0954-3899/39/10/105005.

[7] S. Chatrchyan et al. "Interpretation of searches for supersymmetry with simplified models". In: *Physical Review D* 88.5 (Sept. 2013). ISSN: 1550-2368. DOI: 10.1103/physrevd.88.052017. URL: http://dx.doi.org/10.1103/PhysRevD.88.052017.

[8] G. Aad et al. "Summary of the ATLAS experiment's sensitivity to supersymmetry after LHC Run 1 — interpreted in the phenomenological MSSM". In: *Journal of High Energy Physics* 2015.10 (Oct. 2015). ISSN: 1029-8479. DOI: 10.1007/jhep10(2015)134. URL: http://dx.doi.org/10.1007/JHEP10(2015)134.

[9] V. Khachatryan et al. "Phenomenological MSSM interpretation of CMS searches in pp collisions at $\sqrt{s}$ = 7and 8 TeV". In: *Journal of High Energy Physics* 2016.10 (Oct. 2016). ISSN: 1029-8479. DOI: 10.1007/jhep10(2016)129. URL: http://dx.doi.org/10.1007/JHEP10(2016)129.

[10] Abdelhak Djouadi, Jean-Loïc Kneur, and Gilbert Moultaka. "SuSpect: A Fortran code for the Supersymmetric and Higgs particle spectrum in the MSSM". In: *Computer Physics Communications* 176.6 (Mar. 2007), pp. 426–455. ISSN: 0010-4655. DOI: 10.1016/j.cpc.2006.11.009. URL: http://dx.doi.org/10.1016/j.cpc.2006.11.009.

[11] Carola F Berger et al. "Supersymmetry without prejudice". In: *Journal of High Energy Physics* 2009.02 (Feb. 2009), pp. 023–023. ISSN: 1029-8479. DOI: 10.1088/1126-6708/2009/02/023. URL: http://dx.doi.org/10.1088/1126-6708/2009/02/023.

[12] Matthew W. Cahill-Rowley et al. "The new look pMSSM with neutralino and gravitino LSPs". In: *The European Physical Journal C* 72.9 (Sept. 2012). ISSN: 1434-6052. DOI: 10.1140/epjc/s10052-012-2156-1. URL: http://dx.doi.org/10.1140/epjc/s10052-012-2156-1.

[13] Ursula Laa. *On the coverage of the pMSSM by simplified model results*. 2017. arXiv: 1709.10386 [hep-ph].

[14] P Skands et al. "SUSY Les Houches Accord: Interfacing SUSY Spectrum Calculators, Decay Packages, and Event Generators". In: *Journal of High Energy Physics* 2004.07 (July 2004), pp. 036–036. ISSN: 1029-8479. DOI: 10.1088/1126-6708/2004/07/036. URL: http://dx.doi.org/10.1088/1126-6708/2004/07/036.

[15] W. Porod. "SPheno, a program for calculating supersymmetric spectra, SUSY particle decays and SUSY particle production at e+e colliders". In: *Computer Physics Communications* 153.2 (2003), pp. 275–315. ISSN: 0010-4655. DOI: https://doi.org/10.1016/S0010-4655(03)00222-4. URL: https://www.sciencedirect.com/science/article/pii/S0010465503002224.

[16] W. Porod and F. Staub. "SPheno 3.1: extensions including flavour, CP-phases and models beyond the MSSM". In: *Computer Physics Communications* 183.11 (Nov. 2012), pp. 2458–2469. ISSN: 0010-4655. DOI: 10.1016/j.cpc.2012.05.021. URL: http://dx.doi.org/10.1016/j.cpc.2012.05.021.

[17] Henning Bahl et al. *Precision calculations in the MSSM Higgs-boson sector with FeynHiggs 2.14*. 2019. arXiv: 1811.09073 [hep-ph].

[18] Henning Bahl et al. "Reconciling EFT and hybrid calculations of the light MSSM Higgs-boson mass". In: *The European Physical Journal C* 78.1 (Jan. 2018). ISSN: 1434-6052. DOI: 10.1140/epjc/s10052-018-5544-3. URL: http://dx.doi.org/10.1140/epjc/s10052-018-5544-3.

[19] Henning Bahl and Wolfgang Hollik. "Precise prediction for the light MSSM Higgs-boson mass combining effective field theory and fixed-order calculations". In: *The European Physical Journal C* 76.9 (Sept. 2016). ISSN: 1434-6052. DOI: 10.1140/epjc/s10052-016-4354-8. URL: http://dx.doi.org/10.1140/epjc/s10052-016-4354-8.

[20] T. Hahn et al. "High-Precision Predictions for the LightCP-Even Higgs Boson Mass of the Minimal Supersymmetric Standard Model". In: *Physical Review Letters* 112.14 (Apr. 2014). ISSN: 1079-7114. DOI: 10.1103/physrevlett.112.141801. URL: http://dx.doi.org/10.1103/PhysRevLett.112.141801.

[21] Meikel Frank et al. "The Higgs boson masses and mixings of the complex MSSM in the Feynman-diagrammatic approach". In: *Journal of High Energy Physics* 2007.02 (Feb. 2007), pp. 047–047. ISSN: 1029-8479. DOI: 10.1088/1126-6708/2007/02/047. URL: http://dx.doi.org/10.1088/1126-6708/2007/02/047.

[22] G. Degrassi et al. "Towards high-precision predictions for the MSSM Higgs sector". In: *The European Physical Journal C* 28.1 (May 2003), pp. 133–143. ISSN: 1434-6052. DOI: 10.1140/epjc/s2003-01152-2. URL: http://dx.doi.org/10.1140/epjc/s2003-01152-2.

[23] S. Heinemeyer, W. Hollik, and G. Weiglein. "The masses of the neutral $\mathcal{CP}$ -even Higgs bosons in the MSSM: Accurate analysis at the two-loop level". In: *The European Physical Journal C* 9.2 (June 1999), pp. 343–366. ISSN: 1434-6052. DOI: 10.1007/s100529900006. URL: http://dx.doi.org/10.1007/s100529900006.

[24] S. Heinemeyer, W. Hollik, and G. Weiglein. "FeynHiggs: a program for the calculation of the masses of the neutral -even Higgs bosons in the MSSM". In: *Computer Physics Communications* 124.1 (Jan. 2000), pp. 76–89. ISSN: 0010-4655. DOI: 10.1016/s0010-4655(99)00364-1. URL: http://dx.doi.org/10.1016/S0010-4655(99)00364-1.

[25] F. Mahmoudi. "SuperIso v2.3: A program for calculating flavor physics observables in supersymmetry". In: *Computer Physics Communications* 180.9 (Sept. 2009), pp. 1579–1613. ISSN: 0010-4655. DOI: 10.1016/j.cpc.2009.02.017. URL: http://dx.doi.org/10.1016/j.cpc.2009.02.017.

[26] Philip Bechtle et al. "HiggsSignals: Confronting arbitrary Higgs sectors with measurements at the Tevatron and the LHC". In: *The European Physical Journal C* 74.2 (Feb. 2014). ISSN: 1434-6052. DOI: 10.1140/epjc/s10052-013-2711-4. URL: http://dx.doi.org/10.1140/epjc/s10052-013-2711-4.

[27] P. Bechtle et al. "HiggsBounds: Confronting arbitrary Higgs sectors with exclusion bounds from LEP and the Tevatron". In: *Computer Physics Communications* 181.1 (Jan. 2010), pp. 138–167. ISSN: 0010-4655. DOI: 10.1016/j.cpc.2009.09.003. URL: http://dx.doi.org/10.1016/j.cpc.2009.09.003.

[28] Philip Bechtle et al. *Recent Developments in HiggsBounds and a Preview of HiggsSignals*. 2013. arXiv: 1301.2345 [hep-ph].

[29] Philip Bechtle et al. "HiggsBounds-4: improved tests of extended Higgs sectors against exclusion bounds from LEP, the Tevatron and the LHC". In: *The European Physical Journal C* 74.3 (Mar. 2014). ISSN: 1434-6052. DOI: 10.1140/epjc/s10052-013-2693-2. URL: http://dx.doi.org/10.1140/epjc/s10052-013-2693-2.

[30] Philip Bechtle et al. "Applying exclusion likelihoods from LHC searches to extended Higgs sectors". In: *The European Physical Journal C* 75.9 (Sept. 2015). ISSN: 1434-6052. DOI: 10.1140/epjc/s10052-015-3650-z. URL: http://dx.doi.org/10.1140/epjc/s10052-015-3650-z.

[31] P.A. Zyla et al. "Review of Particle Physics". In: *PTEP* 2020.8 (2020), p. 083C01. DOI: 10.1093/ptep/ptaa104.

[32] Peter Athron et al. "GM2Calc: precise MSSM prediction for $(g-2)$ of the muon". In: *The European Physical Journal C* 76.2 (Feb. 2016). ISSN: 1434-6052. DOI: 10.1140/epjc/s10052-015-3870-2. URL: http://dx.doi.org/10.1140/epjc/s10052-015-3870-2.

[33] Peter Athron et al. *Two-loop Prediction of the Anomalous Magnetic Moment of the Muon in the Two-Higgs Doublet Model with GM2Calc 2*. 2021. arXiv: 2110.13238 [hep-ph].

[34] B. Abi et al. "Measurement of the Positive Muon Anomalous Magnetic Moment to 0.46 ppm". In: *Physical Review Letters* 126.14 (Apr. 2021). ISSN: 1079-7114. DOI: 10.1103/physrevlett.126.141801. URL: http://dx.doi.org/10.1103/PhysRevLett.126.141801.

[35] Sabine Kraml et al. "SModelS: a tool for interpreting simplified-model results from the LHC and its application to supersymmetry". In: *Eur. Phys. J. C* 74 (2014), p. 2868. DOI: 10.1140/epjc/s10052-014-2868-5. arXiv: 1312.4175 [hep-ph].

[36] Federico Ambrogi et al. "SModelS v1.1 user manual: Improving simplified model constraints with efficiency maps". In: *Comput. Phys. Commun.* 227 (2018), pp. 72–98. DOI: 10.1016/j.cpc.2018.02.007. arXiv: 1701.06586 [hep-ph].

[37] Federico Ambrogi et al. "SModelS v1.2: long-lived particles, combination of signal regions, and other novelties". In: *Comput. Phys. Commun.* 251 (2020), p. 106848. DOI: 10.1016/j.cpc.2019.07.013. arXiv: 1811.10624 [hep-ph].

[38] Gaël Alguero et al. "New developments in SModelS". In: *PoS* TOOLS2020 (2021), p. 022. DOI: 10.22323/1.392.0022. arXiv: 2012.08192 [hep-ph].

[39] G. Bélanger et al. "micrOMEGAs$_3$: $A program for calculating dark matter observables$". In: *Computer Physics Communications* 185.3 (Mar. 2014), pp. 960–985. ISSN: 0010-4655. DOI: 10.1016/j.cpc.2013.10.016. URL: http://dx.doi.org/10.1016/j.cpc.2013.10.016.

[40] D. Barducci et al. *Collider limits on new physics within micrOMEGAs4.3*. 2017. arXiv: 1606.03834 [hep-ph].

[41] G. Bélanger et al. "Dark matter direct detection rate in a generic model with micrOMEGAs$_2$.2". In: *Computer Physics Communications* 180.5 (May 2009), pp. 747–767. ISSN: 0010-4655. DOI: 10.1016/j.cpc.2008.11.019. URL: http://dx.doi.org/10.1016/j.cpc.2008.11.019.

A Coverage of the scan

Throughout this section, sampled pMSSM points that are excluded at post-processing are shown separately from the final accepted sample. Points accepted by the McMC but excluded at 95% CL by HiggsBounds (LHC Higgs searches) are shown in purple. Of the remaining points, those excluded at 95% CL by SModels (LHC SUSY searches) are shown in dark blue. And of the remaining points, those excluded at 95% CL by Micromegas (dark matter measurements) are shown in light blue. The green distribution shows the points that are fully accepted after all post-processing steps.

A.1 pMSSM parameters

The distribution of the sampled trilinear couplings (A_t, A_b, and A_l) are shown in Figure 14. The symmetry across 0 shows that the random selection of initial scan points does indeed populate all sign combinations effectively.

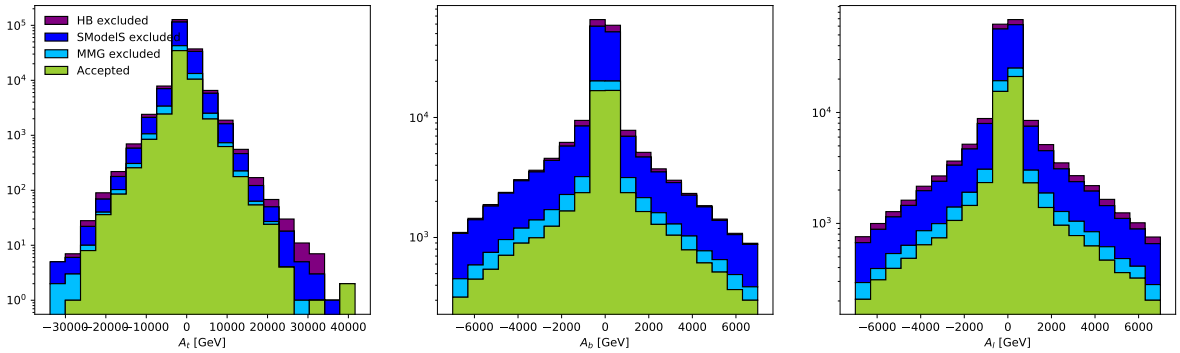

Figure 14: Distribution of the trilinear couplings A_t, A_b, and A_l of sampled pMSSM points.

The distributions of the sampled gaugino mass parameters (μ, M_1, M_2, and M_3) are shown in Figure 15. Again, good symmetry across 0 is observed in μ, M_1, and M_2. The power of LHC SUSY searches is visible at low values of these mass parameters, where the SModelS exclusion rules out the majority of points accepted by the McMC.

The sampled values of slepton mass parameters are shown in Figure 16 for left-handed (left) and right-handed (right) sleptons. The peak at low values of the smuon/selectron mass corresponds to those points with large Δa_μ. These are largely excluded by SModelS.

The sampled squark mass parameters are shown in Figure 17: the left column shows the right-handed up-type, the center column shows the right-handed down-type, and the right column shows the left-handed squark masses. Again, LHC searches have been able to exclude much of the parameter space at low squark masses, as showwn by the SModelS exclusion.

The pMSSM Higgs paramters, the mass of the heavy Higgs boson M_A and $\tan\beta$, are shown in Figure 18. HiggsBounds, which includes dedicated LHC searches for the decay of the heavy Higgs, and SModelS exclude all points with $M_A < XXX$ GeV.

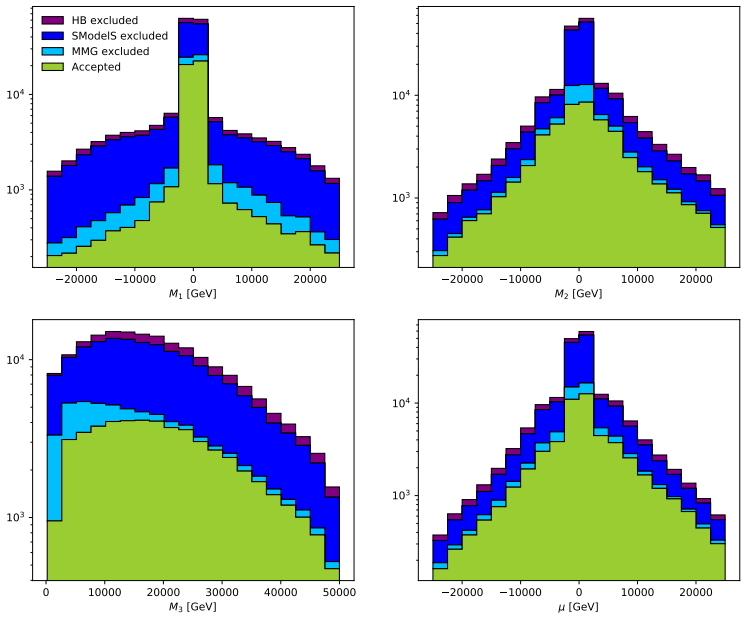

Figure 15: Distribution of the gaugino mass parameters M_3, M_1, M_2, and μ of sampled pMSSM points.

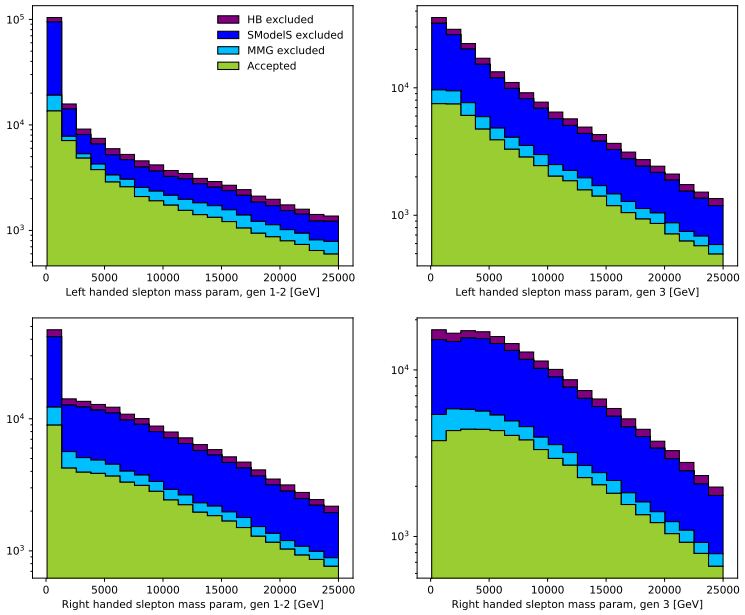

Figure 16: Distribution of slepton mass parameters $m_{\tilde{L}^{1,2}}$, $m_{\tilde{L}^3}$, $m_{\tilde{R}^{1,2}}$, and $m_{\tilde{R}^3}$ of sampled pMSSM points.

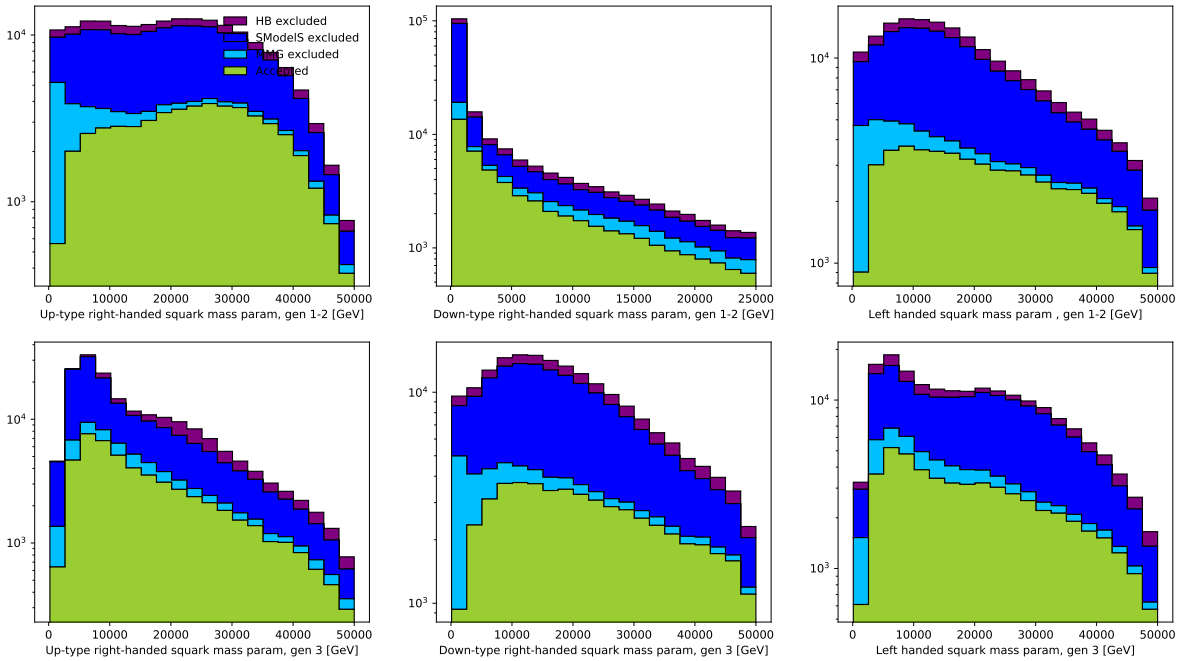

Figure 17: Distribution of squark mass parameters (left) $m_{\tilde{u}^{1,2}}$, $m_{\tilde{u}^3}$, (center) $m_{\tilde{d}^{1,2}}$, $m_{\tilde{d}^3}$, (right) $m_{\tilde{q}^{1,2}}$, $m_{\tilde{q}^3}$ of sampled pMSSM points.

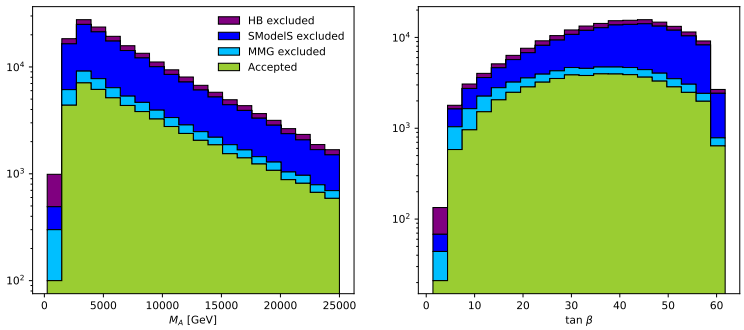

Figure 18: The sampled mass of the heavy Higgs boson M_A (left), and $\tan\beta$ (right) for the sampled pMSSM points.

A.2 Sparticle masses

This section shows the distributions of sparticle masses of the sampled pMSSM points.

Figure 19 shows the slepton masses, Figure 20 shows the sbottom and stop quark masses, and Figure 21 shows the gluino mass. The neutralino masses are shown in Figure **??**.

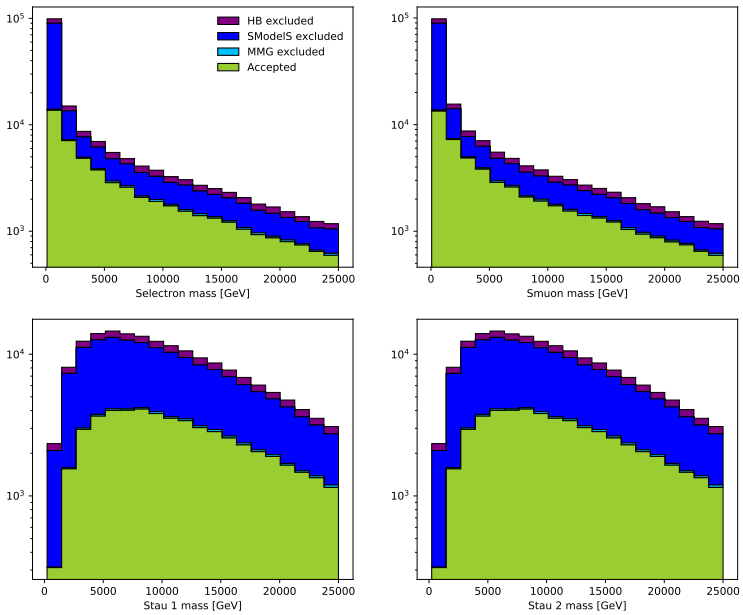

Figure 19: Slepton masses

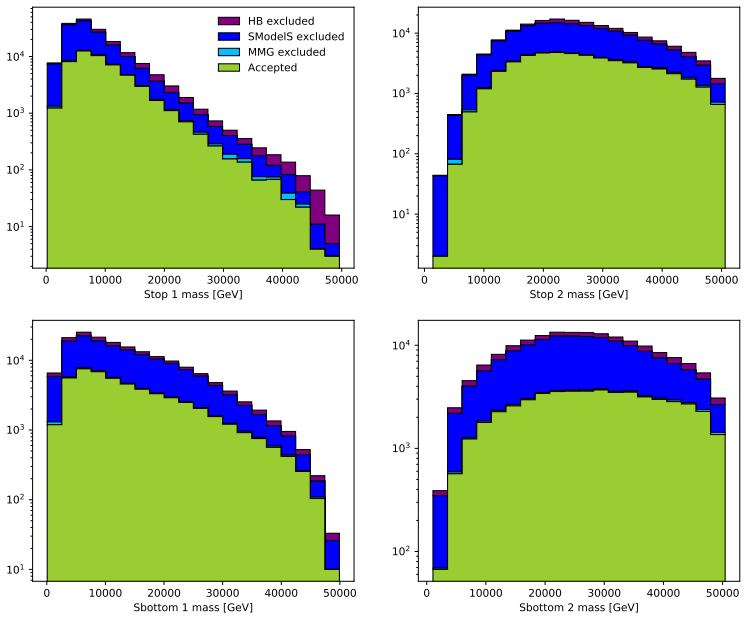

Figure 20: Heavy squark masses

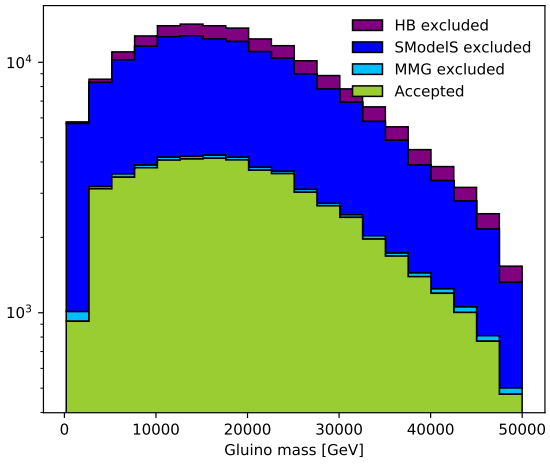

Figure 21: Gluino mass

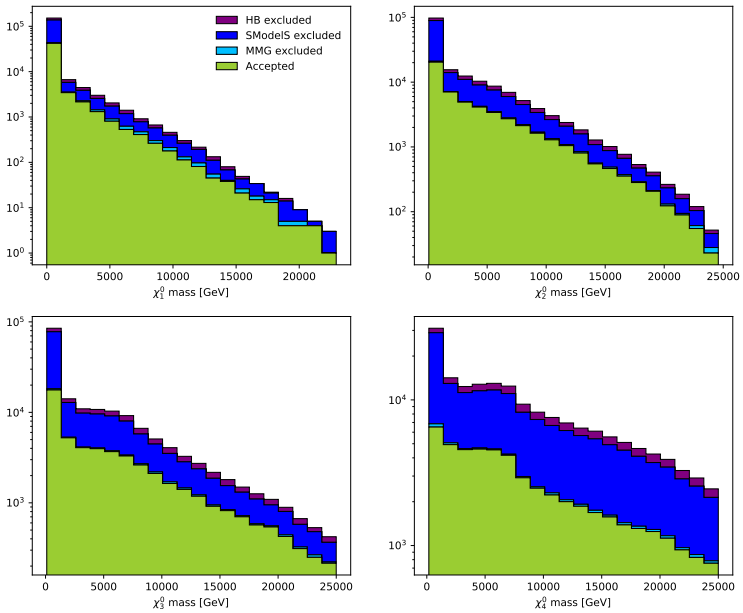

Figure 22: Neutralino masses

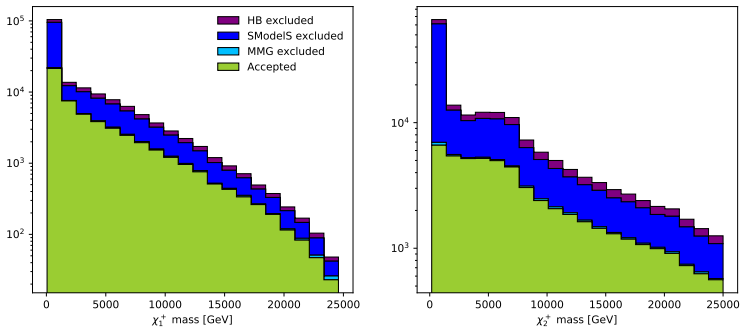

Figure 23: Chargino masses